The effect of jaw curvature on composite crushing performance: how do stingrays eat shells?

Matthew A. Kolmann[1]

Functional Morphology & Ecology of Fishes 2014
Summer 2014

[1] University of Toronto, Toronto, ON Canada M1C 1A4

Contact Information:

Matthew A. Kolmann, MSc.
Ecology & Evolutionary Biology
University of Toronto
1265 Military Trail

Toronto ON M1C 1A4
matthew.kolmann@mail.utoronto.ca

Keywords: Myliobatidae, durophagy, rapid prototyping, fracture, performance

INTRODUCTION

Durophagous animals are equipped with myriad morphological adaptations for consuming durable prey. Convergent traits for processing hard prey generally include robust feeding musculature, cyclical loading patterns for crushing biological composites, reinforced skeletons, and an array of specialized tooth designs (Van Valkenburgh 1988; Summers, 2000; Summers et al., 2003; Huber et al., 2005). Molariform teeth are well-known in mammals, but cusped and even concave tooth shapes are present in durophagous taxa (Erickson et al. 2012; Crofts and Summers, 2014). In some durophagous stingrays (Family Myliobatidae), the teeth are fused, forming paired (upper and lower jaw) occlusal surfaces. Individual teeth interlock to form this tooth module. As in other elasmobranchs, teeth in these rays are conveyed anteriorly (or labially) as they wear and are eventually shed (Reif et al., 1978). These myliobatid stingrays include the eagle (Aetobatinae), bat (Myliobatinae), cownose (Rhinopterinae), and devil (Mobulinae) rays (Aschliman et al., 2012; Aschliman, 2014). These rays generally prey on bivalves, gastropods, and crustaceans while planktivory in mobulines is considered a derived trait (Ajemian & Powers, 2012; Ajemian et al. 2012; Adnet et al., 2012; Aschliman, 2014).

From a putative durophagous ancestor, the resultant skeletal morphologies of these taxa greatly differ in terms of shape and size. The prevalence of isolated myliobatid teeth in the fossil record, in addition to intact, whole tooth modules has resulted in classification of many extinct durophagous rays (Claeson et al., 2010). The cartilaginous skeleton of elasmobranchs, due to its low mineral content, infrequently fossilizes, making fossil teeth essential to understanding the systematic relationships of existing taxa (Whitenack and Gottfried, 2010; Claeson et al., 2010; Adnet et al., 2014). However, the histological and biomaterial characterization of elasmobranch teeth has been a hotly-debated topic for over a century (Whitenack et al., 2010). Numerous functional and systematic hypotheses have been posited based either on the macro- or micro-structure of cartilaginous fish teeth (Croft and Summers, 2014). Understanding which physical properties, particularly shape, contribute to function (if at all), is imperative to understanding the ecology of both extant and extinct animals.

Myliobatid rays are externally similar, but with drastic differences evident between taxa in the shape of the jaws and teeth (Summers, 2000; Kolmann et al., 2014). Eagle rays have a drastically protruding lower jaw (Meckel's cartilage) composed of chevron-shaped teeth. The upper jaw (palatoquadrate) teeth of *Aetobatus*, as well as most myliobatids, are squat and generally hexagonal, with tooth size decreasing medially to laterally (Summers, 2000). The occlusal surface of these rays is slightly domed, with the upper and lower tooth plates differing in their degree of curvature, from planar to rounded arcs. Whether or not the curvatures of the tooth plate modules have any functional significance regarding feeding, prey excavation, or other behaviors, is unknown. Although myliobatids are thought to have slower tooth replacement rates than

other elasmobranchs, the biomechanical attributes of this high-performance, high-replacement biological system is an interesting subject for biomimetic applications.

Here we take a reductionist approach to understanding how the curvature of the tooth plate module affects crushing performance, and by proxy, whole animal performance (Arnold, 1983). The nature of skeletal material and structural properties (on behalf of predator AND prey) are exceedingly complex. Controlling for one property in order to infer the other provides a unique opportunity to study the biomechanical evolution of the materials involved in feeding behaviors. Rapid prototyping and other additive constructive processes can form an inexhaustible supply of shells with identical or near-identical material and structural properties, while maintaining a standard shell shape, which can be scaled to any size (Crofts and Summers, 2014). Here I will address several questions and objectives: (1) whether crushing printed shells and ceramic tubes can allow us to infer basic principles of composite crushing performance by differentially-curved structures (jaws). I will do this by comparing the forces necessary to crush these materials, using different jaw shapes. (2) I will vary both simulated prey size, as well as jaw shape, to explore whether jaw curvature lends differential crushing performance at various prey sizes. I hypothesize that disparity in the curvature between the upper and lower jaw among species will drive differential crushing performance on differently-sized shells (Figure 1). Specifically, having a more rounded jaw coupled with a more occlusal surface will result in higher crushing performance at larger shell sizes. Higher crushing performance of smaller shells will be seen in animals, like *Rhinoptera*, in which both jaws are comparatively rounded. This could be due to concentrating forces to a smaller unit area, thereby increasing bite pressure concentrations regionally across the shell. Larger rays, such as *Aetobatus* may use a different strategy, whereby total pressure across a large, flat tooth plate is antagonized with a curved upper jaw, which increases crushing performance on larger shells.

METHODS

Whole specimens of *Aetomylaeus nichofii*, *Aetobatus narinari*, *Myliobatis tobejei*, and *Rhinoptera bonasus* were obtained from museum collections. These specimens underwent computed tomography (ct) scanning with a 16-slice medical grade Siemens RS SOMATOM Sensation (MDCT-16) with 0.75-mm slice thickness and helical-spiral scans for a previous study (Dean *et al*. 2007). Specimen information can be found in the appendix. Specimens were wrapped in alcohol saturated cheesecloth and sealed in large Ziploc bags, allowing several specimens to be scanned simultaneously. Scans were reconstructed as 8-bit TIFF stacks and rendered as three-dimensional visualizations using Amira software (v. 5.2.2, Visage Imaging, Inc.). The upper and lower jaws (palatoquadrate and Meckel's cartilage, respectively) were segmented separately from the rest of the body. The medial sagittal section of each jaw was manually traced in Adobe Illustrator CS (Adobe Systems, Inc.). These two-dimensional images were then extruded (extended into the z-axis), resulting in four pairs of three-dimensional jaw shapes of 40mm standard width in 123D Design (v. 1.4.51, Autodesk, Inc.). These simplified jaw shapes were cropped to include only the relevant occlusal surface. The occlusal surface was determined by examining the pattern of wear on specimen tooth plates. These jaw shapes were exported as .stl files into SprutCAM7 Pro (v. 7.1.5, Sprut Technologies, Inc.), a program for CNC (computer numerical controlled) milling. Using a 4-axis mill

(Tormach CNC1000), jaw pairs were fashioned from 6061-grade aluminum stock, lightly sanded with a belt sander, and then polished.

Aluminum jaw replicas were threaded and attached to a mechanical loading frame (Synergie 100, MTS Systems Corp.) coupled to a 500N load cell (Figure 3). Two types of materials were subjected to materials testing, ceramic filter media (FluVal BioMax filter rings, Hagen, Inc.) and 3D-printed replica shells (ZPrinter 310, ZCorporation, Inc.) of *Nucella lamellosa*. These materials were chosen to represent basic shapes with only slightly-varying material and structural properties, contrary to what exists in natural systems (i.e. actual gastropods). Replica shells were printed in plaster, hardened using a solution of magnesium chloride and water, and then placed in a vacuum heater for 12hrs to dry and harden. These printed shells were scaled appropriately at 0.5cm intervals, giving three size classes, 1.0cm, 1.5cm, and 2.0cm (spire length). Ceramic tube dimensions were measured using ImageJ (v. 1.40, National Institute of Health, Bethesda, MD) prior to crushing.

Ceramic tubes and shells were placed at the same occlusal point in each trial, with their orientation to the jaw (with operculum or tube opening) facing either laterally or linguo-labially (in printed shells, the spire was set facing lingually). Shells were crushed using a compressive loading regime of 2.7mm/s. Peak load (N) and yield load (N) were determined from stress/strain curves generated by TestWorks4 software (v. 4.08, MTS Systems Corp.) and recorded after each trial. In order to test for the greatest effect of jaw curvature on crushing performance, *Aetomylaeus* and *Rhinoptera* jaws were used exclusively for the printed shell trials. Shells were sized at 1 mm, 1.5 mm, 2 mm, 2.5 mm, and 3 mm in spire length.

Analysis of covariance (ANCOVA) was used to explore the relationship between jaw shape and crushing performance, with respect to prey orientation and size. All analyses were run in R (v. 2.15.0, www.theRproject.org).

RESULTS

Ceramic Tubes

There were no significant differences between taxa in peak load generation while crushing ceramic tubes (Figure 4). The width (first largest axis of tube cross-section) of the ceramic tubes was strongly related to peak load (F-value: 11.321; Pr > F: 0.0011), as was tube length (F-value: 4.885; Pr > F: 0.0295). Yield load was significantly correlated with tube width (F-value: 9.762; Pr > F: 0.00236) and length (F-value: 4.976; Pr > F: 0.02802). Various interactions between taxon, orientation, and tube dimensions were also found to be significant (Table 2; Taxon:Orientation, Tube Depth: Orientation, Taxon:Length, Taxon:Width:Depth). The interaction between all these variables, yield load and taxon was also found to be significant (F-value: 2.115; Pr > F: 0.0376). Orientation of prey on the occlusal surface in a labio-lingual direction resulted in *Aetomylaeus* and *Aetobatus* exhibiting lower loadings (peak and yield). The opposite pattern was seen in *Myliobatis* and *Rhinoptera*, where lateral prey orientation resulted in lower loadings (Figures 5 & 6).

Printed Shells

Average loadings and standard deviations are reported in Table 2. Shells consistently showed crack formation at the base of the spire in almost all trials. Crack

propagation continued dorsally along the spire suture, paralleling the shell aperture (Figure 7). This pattern was repeated across shells invariant to shell size. Forces to fracture (peak load and yield load) were significantly different between *Aetomylaeus* and *Rhinoptera* for small shells. Peak load and yield load showed similar trends using ANCOVAs, whereby shell size was strongly significant whether it was included as a factor (peak: F-value: 22.952; Pr > 6.98e-11, yield: F-value: 17.248; Pr > 8.99e-09) or interaction (peak: F-value: 21.005; Pr > F: 2.84e-10, yield: F-value: 15.975; Pr > F: 2.54e-08). The interaction between species and shell size class is also significant (F-value: 3.2584; Pr > F: 0.02567). Although *Aetomylaeus* and *Rhinoptera* overall share similar patterns of crushing performance, the variances are different and the outright performance when crushing small shells is divergent (Figures 8 & 9).

DISCUSSION

Here I show that jaw shape has little overall effect on crushing performance with regards to generalized prey shapes such as composite cylinders and printed shells. However, size differences in the prey itself, and presumably the predator as well, can produce nuanced differences in feeding performance. Yield load is presumably more biologically relevant to feeding interactions in that initial injury and in this case, first fracture of the prey exoskeleton is particularly relevant to prey processing. As suggested for the musk turtle, *Sternotherus minor* (Pfaller et al. 2009), initial crack propagation is critical to winnowing behaviors, which iteratively increase point-loadings and stress concentrations on composite shells until catastrophic failure is induced across the whole structure. In this manner animals with seemingly insufficient bite forces to outright fail composite skeletons can still feed above their raw muscular performance. In this study however, prey failure forces stood well within bite forces estimated for at least one of the species studied, *Rhinoptera bonasus* (Kolmann, 2012; Kolmann et al., *in prep*) as well as anecdotal values for others, i.e. *Myliobatis freminvillei* and *Aetobatus narinari* (Kolmann and Grubbs, unpublished).

Winnowing behaviors involve successive handling and reorientation of prey, followed by iterative crushing events. Interestingly, the orientation of our ceramic tubes highlighted differences in crushing performance across taxa. Labio-lingual orientation of shells promoted lower yield and peak forces in rays which had a higher disparity of jaw curvature (i.e., one curved and one planar, or near curved jaws – *Aetobatus* and *Aetomylaeus*). The opposite trend was seen in *Myliobatis* and *Rhinoptera*, whereby a lateral orientation of prey on more curved jaws promoted lower peak and yield loads. In an anterior-posterior (labio-lingual) orientation on planar jaws, the smaller shape aspect would be contacted by the stress-concentrating curvature of the upper jaw along the midpoint of the tube. In the opposite scenario, where the tube is positioned laterally, the single largest face of prey is contacting the tooth surface. This suggests that pressure and surface area relationships are in play, whereby a curved surface minimizes contact and therefore maximizes pressure on the prey item. Contrastingly, rays with two curved surfaces are potentially mitigating this scenario by reducing the contact area between the curved occlusal surface and the curved prey carapace. This strategy could serve to increase force application over a smaller area, increasing pressure and strain on the prey surface. An animal while winnowing would seemingly suffer both these scenarios, so the relevance of using one strategy over another, in terms of jaw curvature, is unclear.

With regard to shell size, our small sample size and the use of only two "species" precludes our ability to determine much. However, for both *Rhinoptera* and *Aetomylaeus* we find that medium-sized shells have a lower load (both peak and yield) than small and large shells. This finding is somewhat consistent with our hypotheses that taxa would fall into either generalist or specialist categories – with one jaw curvature being ideal at breaking a given size range of shells. Both species showed similar results; however the magnitude of crushing efficiency was different between the two taxa, with *Aetomylaeus* having higher performance at all shell sizes than *Rhinoptera*, particularly at small shell sizes.

Durophagy (consuming shelled prey) is thought to be a radical departure from other feeding strategies. This is due in part to the specialized morphological features posited as critical to high-performance feeding. The primary challenge facing juvenile durophages is the mechanical processing of robust prey, a difficulty when juveniles are at a performance disadvantage when competing with adults. Morphologically specialized anatomies have been tied to specializations in behavior (in this case, feeding and diet). Liem (1980) however has proposed that specialist consumers are only truly specialized in times where potential prey is particularly limited (e.g. in seasonally variable or particularly patchy habitats). Some tenets of optimal foraging theory may be ignored in these cases, in as much as specialist predators will not be acting at their most optimum at all times. Feeding behavior in durophagous taxa has generally been treated using an optimal perspective, where these animals are feeding on the largest, toughest prey possible, in order to maximize their energetic forays. These claims are difficult to validate experimentally or observationally from either gut-content (prey size is difficult to determine) or prey-handling (behavioral motivation; confounded by captivity) studies. Although foraging theory has its place, more often than not, either at the fault of morphologists or those who study bioenergetics, the influence of competing fitness selection can muddy the form/function continuity. Barel (1988) championed constructional morphology, which sought to examine the inclusive effects of multiple structures on optimum function. Our results suggest that there does not seem to be a direct relationship between crushing performance and jaw shape. Differences in crushing performance may be due to muscular or physiological adaptations, rather than outright shape differences in the skeletal system. Another potential perspective into why jaw performance does not seem to change with jaw shape is a constructional one. Bat rays typically have deeper heads and taller overall gapes, than rhinopterines, which have restricted vertical gapes. Aetobatines and myliobatines seem to consume large-bodied gastropods, with rhinopterines choosing smaller, squatter mollusks, such as *Mya arenaria* (Gray et al. 1997; Yamaguchi et al 2005; Jardas et al. 2007; Collins et al., 2007; Ajemian et al. 2012). While the curvature of the upper jaw seems consistent across taxa, a planar or curved lower jaw seems highly variable.

ACKNOWLEDGEMENTS

I thank Adam Summers and Nathan Lovejoy for providing funding for me to attend this course, as well as funding from World Wildlife Fund Guianas. I thank Adam again, as well as Stephanie Crofts, Stacy Farina, and Misty Paig-Tran for trouble-shooting issues regarding experimental design, software quirks, hardware malfunctions,

and theoretical considerations. JJ Lomax in particular was invaluable when coming to working on aluminum milling, as well as the rest of the FHL maintenance and shop team. Mason Dean, Misty Paig-Tran, Joe Bizzarro, and Ronald Seidel were instrumental in scanning and segmenting many batoid ct scans prior to this project. Cassandra Donnatelli and Matthew Tietbohl were instrumental in collecting live mollusks for this project. I also thank all my classmates at Friday Harbor Labs for providing an enthusiastic, titillating work environment throughout the duration of our tenure here. Friday Harbor Labs has provided an excellent facility for learning and experimentation. Finally, I thank Sigma Xi and Florida State Coastal and Marine Laboratory for funding which related to the gathering of preliminary data leading to this project idea.

LITERATURE

Adnet, S., Cappetta, H., Guinot, G. and Notarbartolo di Sciara, G. (2012). Evolutionary history of the devil rays (Chondrichthyes: Myliobatiformes) from fossil and morphological inference. *Zool J Linnean Soc*. **166**, 132-159.

Ajemian, M.J. and Powers, S.P. (2012). Habitat-specific feeding by cownose rays (*Rhinoptera bonasus*) of the northern Gulf of Mexico. *Environ Biol Fishes*. **95**, 79-97.

Ajemian, M.J., Powers, S. P. and Murdoch, T.J.T. (2012). Estimating the potential impacts of large mesopredators on benthic resources: integrative assessment of spotted eagle ray foraging ecology in Bermuda. *PLoS Biol*. **7**(7): e40227.

Arnold, S.J. (1983). Morphology, performance, and fitness. *Amer Zool*. **23**(2): 347-361.

Aschliman, N.C., Nishida, M., Inoue, J.G., Rosana, K.M. and Naylor, G.J.P. (2012). Body plan convergence in the evolution of skates and rays (Chondrichthyes: Batoidea). *Mol Phylogenet Evol*. **63**, 28-42.

Barel, C. D. N. "Form-relations in the context of constructional morphology: the eye and suspensorium of lacustrine cichlidae (Pisces, Teleostei)." *Netherlands journal of zoology* 34.4 (1983): 439-502.

Collins, A.B., M.R. Heupel, R.E. Hueter, and P.J. Motta. (2007). Hard prey specialists or opportunistic generalists? An examination of the diet of the cownose ray, *Rhinoptera bonasus*. *Mar Freshwater Res*. **58**, 135–144.

Crofts, S. Summers, A.P. (2014). How to best smash a shell: the effect of tooth shape on crushing load. J Roy Soc Int.

Gray, A. E., Mulligan, T. J., and Hannah, R. W. (1997). Food habits, occurrence and population structure of the bat ray, *Myliobatis californica*, in Humboldt Bay, California. *Environ Biol Fishes*. **49**, 227–238.

Liem, C. (1980). Adaptive Significance of Intra- and Interspecific Differences in the Feeding Repertoires of Cichlid Fishes. Integrative and Comparative Biology.

Jardas, I., Santic, M., and Pallaoro, A. (2004). Diet composition of the eagle ray, *Myliobatis aquila* (Chondrichthyes: Myliobatidae), in the eastern Adriatic Sea. *Cybium*. **28**(4), 372-374.

Pfaller, J.B., Gignac, P.M., and Erickson, G.M. (2011). Ontogenetic changes in jaw-muscle architecture facilitate durophagy in the turtle *Sternotherus minor*. *J Exp Biol*. **214**, 1655-1667.

Schwartz, F.J. (1990). Mass migratory congregations and movements of several species of cownose rays, Genus *Rhinoptera*: a world-wide review. *J Elisha Mitchell Sci. Soc*. **106**(1), 10-13.

Summers, A. P. (2000). Stiffening the stingray skeleton – an investigation of durophagy in myliobatid stingrays (Chondrichthyes, Batoidea, Myliobatidae). *J Morphol*. **243**, 113–126.

Yamaguchi, A., Kawahara, I. and Ito, S. (2005). Occurrence, growth and food of longheaded eagle ray, *Aetobatus flagellum*, in Ariake Sound, Kyushu, Japan. *Env Biol Fishes*. **74**, 229-238.

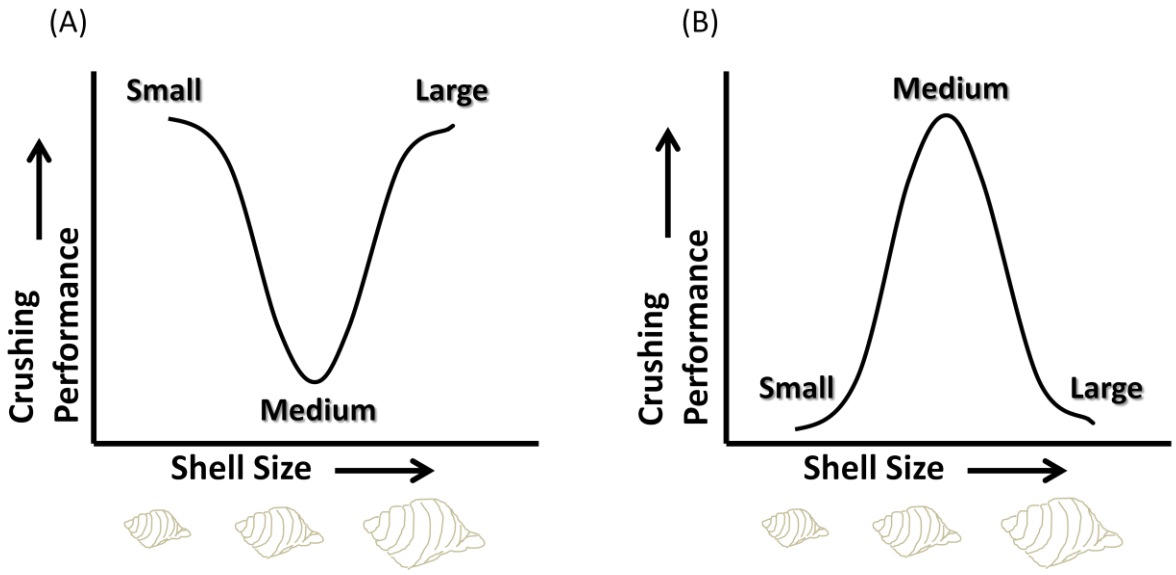

Figure 1: Hypotheses regarding size-effects on crushing performance. (A): "Specialist" model – crushing performance increases at small or large sized-shells, depending on species. (B): "Generalist" model – crushing performance is maximized at intermediate shell sizes.

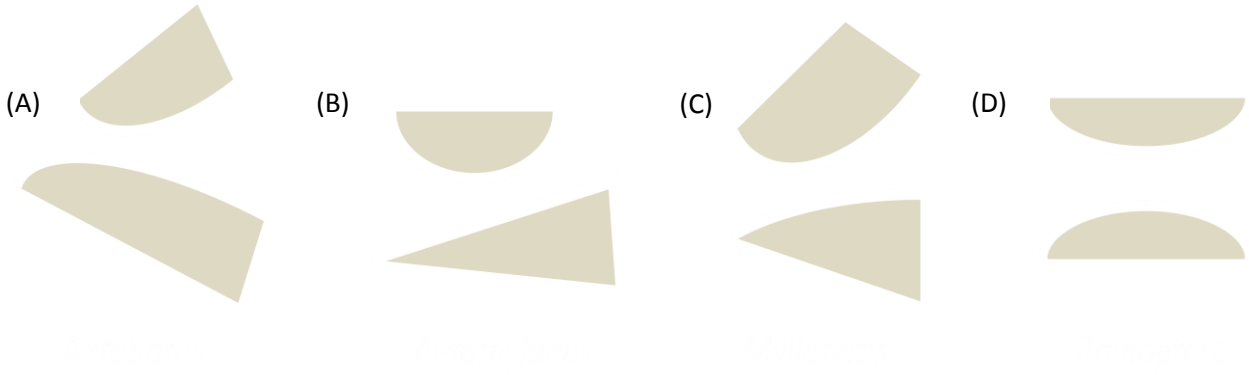

Figure 2: Representative jaw cross-sections for aluminum milling. (A): *Aetobatus narinari*,
(B): *Aetomylaeus nichofi*, (C): *Myliobatis tobejei*, (D): *Rhinoptera bonasus*.

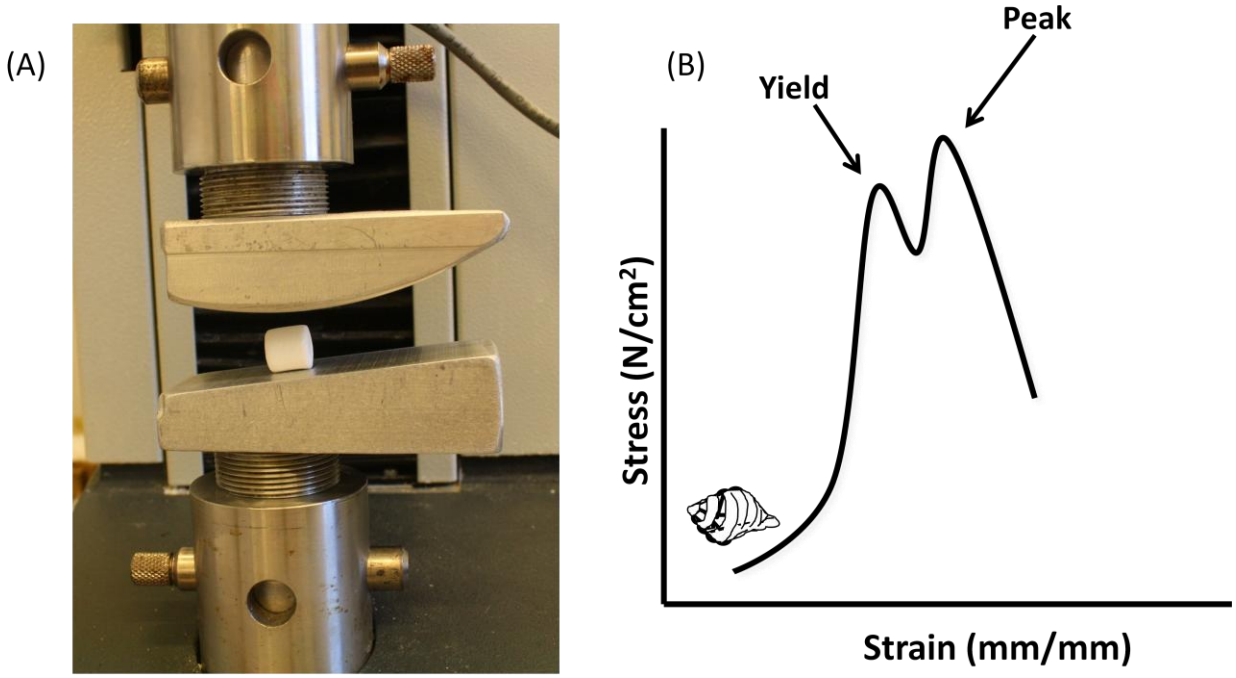

Figure 3: Mechanical loading frame assumptions and aluminum-milled jaw apparatus.
(A): Aluminum jaw apparatus of *Aetomylaeus* with ceramic tube at occlusal surface. (B): Generalized stress/strain curve showing yield and peak load points.

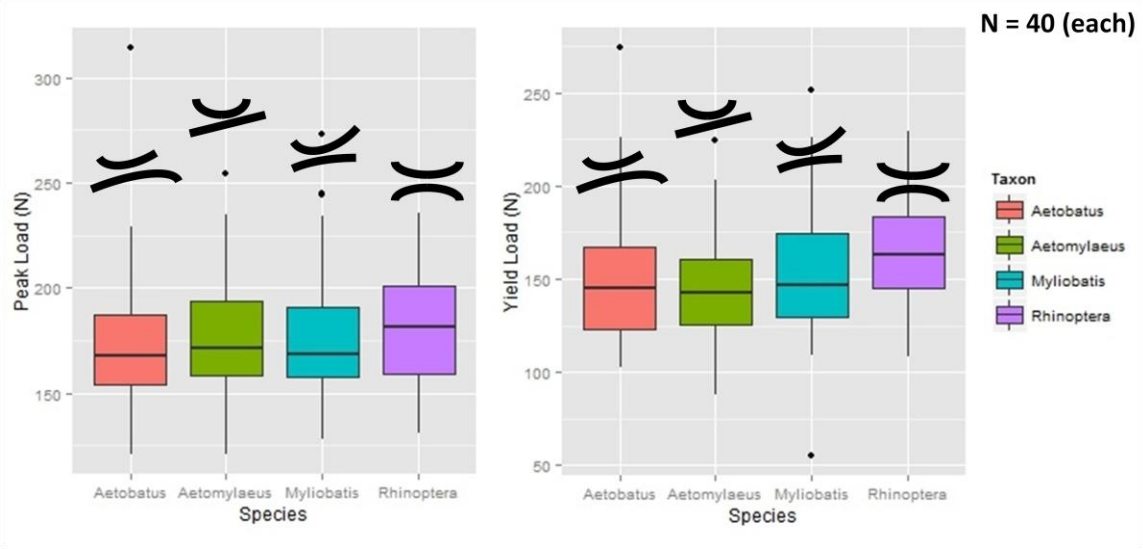

Figure 4.

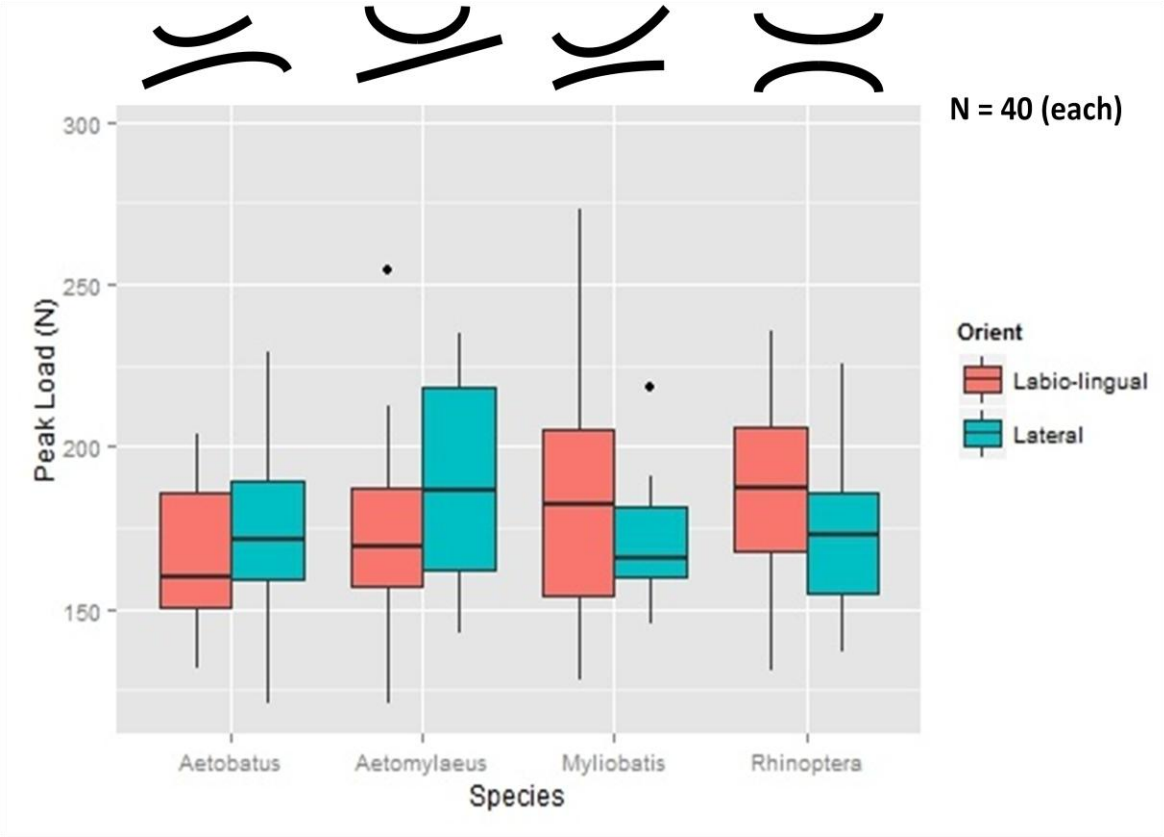

Figure 5.

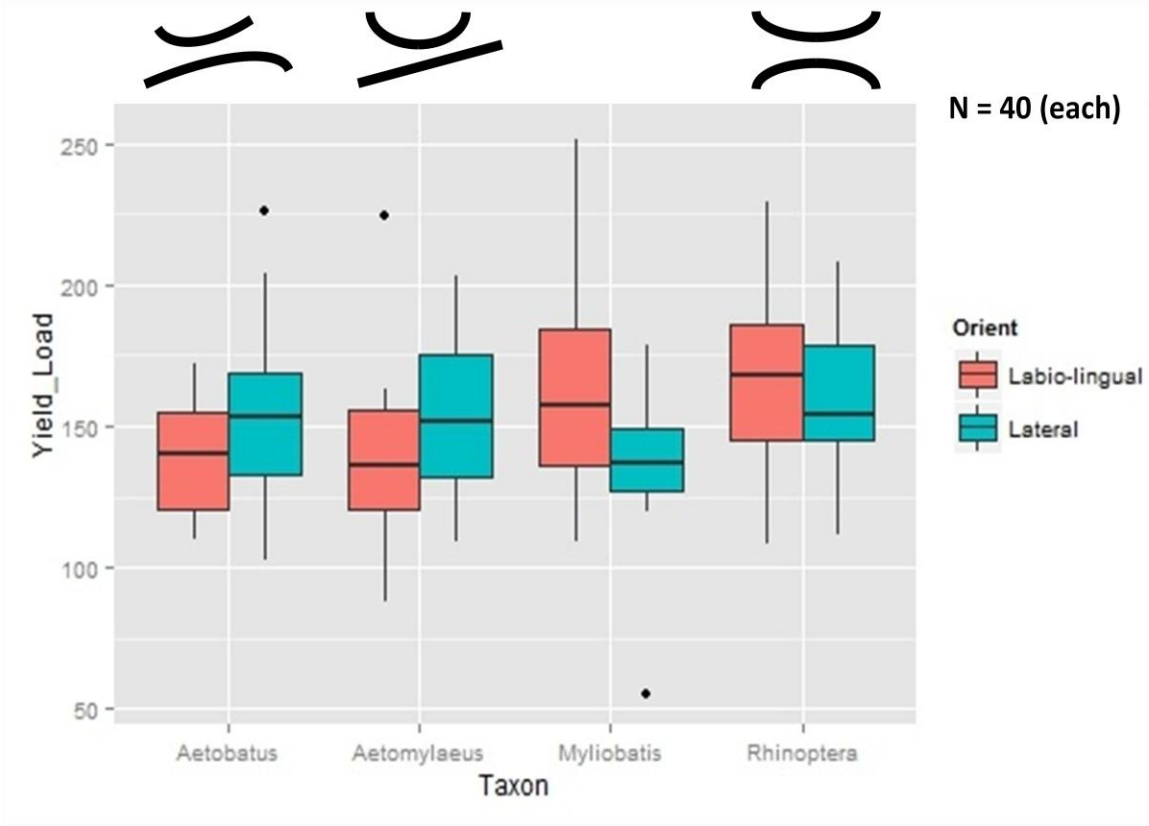
N = 40 (each)
Yield_Load
250
200
150
100
50
Aetobatus
Aetomylaeus
Myliobatis
Rhinoptera
Taxon
Orient
Labio-lingual
Lateral

Figure 6.

Figure 7: Photo of consistent structural failure patterns (crack propagation) in prototyped shells.

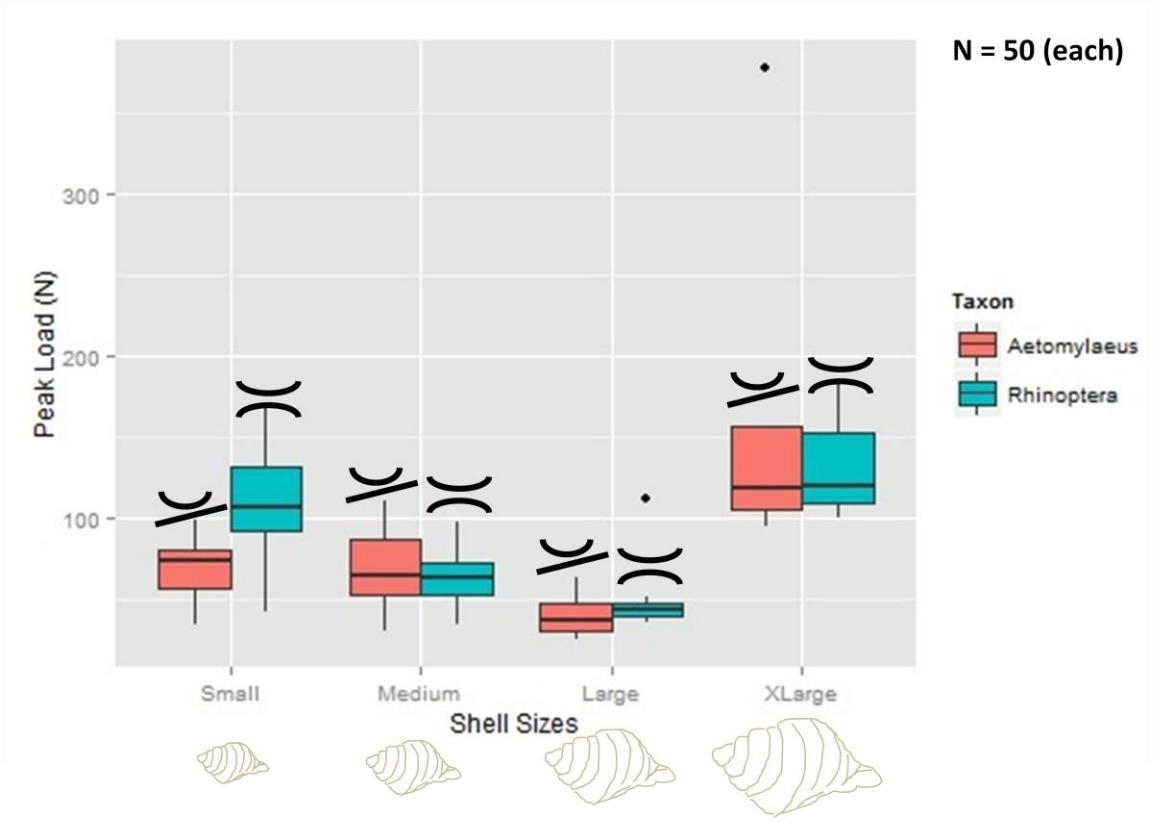

Figure 8.

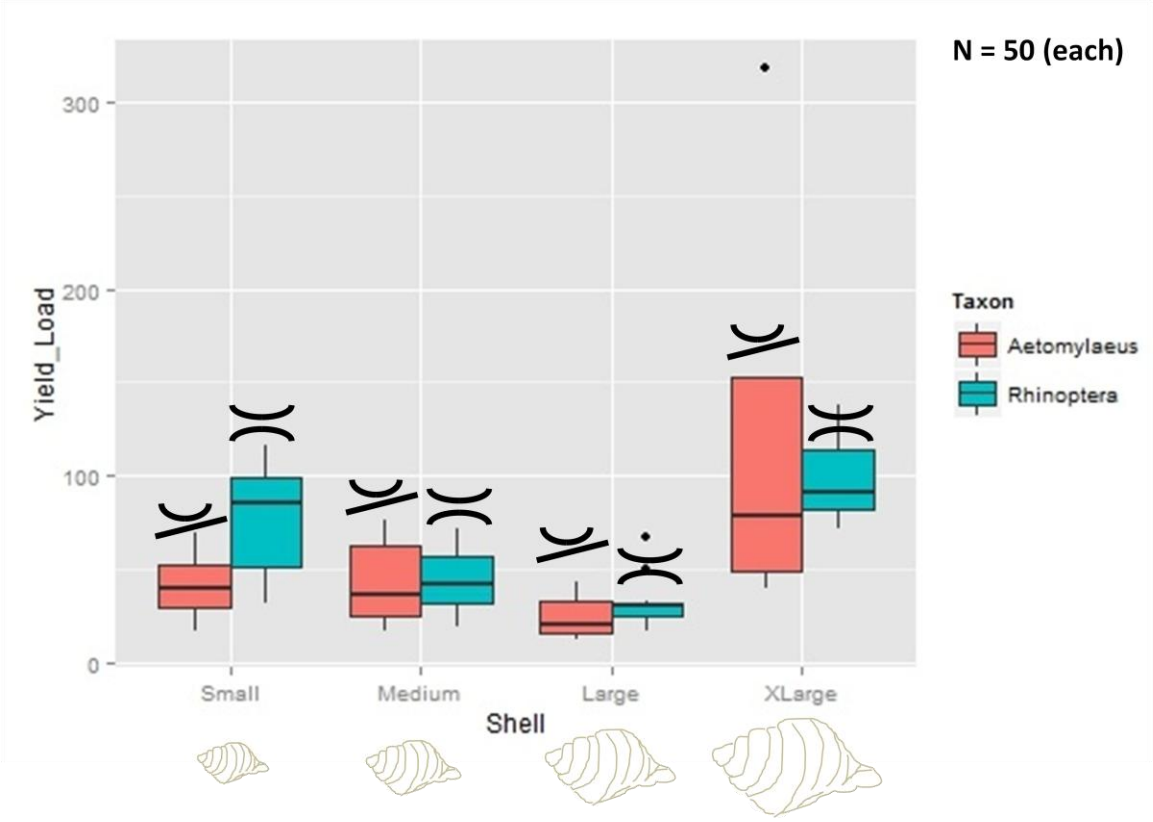

Figure 9.

Table 1. Summary statistics for ceramic tubes.

summary(aov(Peak_Load~Taxon+Length+Width+Depth+Orient+Occlusion))

	Df	Sum Sq	Mean Sq	F value	Pr(>F)	
Taxon	3	698	233	0.246	0.86397	
Length	1	3552	3552	3.758	0.05442	.
Width	1	8234	8234	8.709	0.00367	**
Depth	1	47	47	0.050	0.82324	
Orient	1	1	1	0.001	0.97774	
Residuals	152	143702	945			

Signif. codes: 0 ‘***’ 0.001 ‘**’ 0.01 ‘*’ 0.05 ‘.’ 0.1 ‘ ’ 1

> summary(aov(Peak_Load~Taxon*Length*Width*Depth*Orient*Occlusion))

	Df	Sum Sq	Mean Sq	F value	Pr(>F)	
Taxon	3	698	233	0.320	0.8109	
Length	1	3552	3552	4.885	0.0295	*
Width	1	8234	8234	11.321	0.0011	**
Depth	1	47	47	0.065	0.7992	
Orient	1	1	1	0.001	0.9746	
Taxon:Length	3	4810	1603	2.205	0.0925	.
Taxon:Width	3	3293	1098	1.509	0.2171	
Length:Width	1	166	166	0.228	0.6343	
Taxon:Depth	3	3535	1178	1.620	0.1897	

```
Length:Depth                 1   1208    1208   1.661 0.2006
Width:Depth                  1     81      81   0.112 0.7390
Taxon:Orient                 3   3574    1191   1.638 0.1857
Length:Orient                1   1067    1067   1.467 0.2287
Width:Orient                 1   1183    1183   1.627 0.2052
Depth:Orient                 1   1607    1607   2.210 0.1404
Taxon:Length:Width           3   6917    2306   3.170 0.0278 *
Taxon:Length:Depth           3   3553    1184   1.628 0.1879
Taxon:Width:Depth            3   6013    2004   2.756 0.0466 *
Length:Width:Depth           1    329     329   0.452 0.5031
Taxon:Length:Orient          3    863     288   0.396 0.7565
Taxon:Width:Orient           3   4026    1342   1.845 0.1442
Length:Width:Orient          1     19      19   0.027 0.8703
Taxon:Depth:Orient           3   2488     829   1.140 0.3368
Length:Depth:Orient          1   2107    2107   2.897 0.0920 .
Width:Depth:Orient           1   5012    5012   6.892 0.0101 *
Taxon:Length:Width:Depth     3   7981    2660   3.658 0.0151 *
Taxon:Length:Width:Orient    3   1013     338   0.464 0.7078
Taxon:Length:Depth:Orient    3   2763     921   1.266 0.2904
Taxon:Width:Depth:Orient     3   5032    1677   2.307 0.0815 .
Length:Width:Depth:Orient    1   2858    2858   3.930 0.0503 .
Taxon:Length:Width:Depth:Orient  3   2387     796   1.094 0.3555
Residuals                   96  69818     727
---
Signif. codes:  0 ‘***’ 0.001 ‘**’ 0.01 ‘*’ 0.05 ‘.’ 0.1 ‘ ’ 1
> summary(aov(Peak_Load~Taxon:Length:Width:Depth:Orient:Occlusion))
                                  Df Sum Sq Mean Sq F value Pr(>F)
Taxon:Length:Width:Depth:Orient:Occlusion   8   7798   974.7   0.992  0.445
Residuals                                 151 148437   983.0
>
> ##
> summary(aov(Yield_Load~Taxon+Length+Width+Depth+Orient+Occlusion))
            Df Sum Sq Mean Sq F value  Pr(>F)
Taxon        3   6020    2007   1.982 0.11910
Length       1   3781    3781   3.734 0.05517 .
Width        1   7417    7417   7.325 0.00758 **
Depth        1    133     133   0.131 0.71805
Orient       1     47      47   0.047 0.82919
Residuals  152 153924    1013
---
Signif. codes:  0 ‘***’ 0.001 ‘**’ 0.01 ‘*’ 0.05 ‘.’ 0.1 ‘ ’ 1
> summary(aov(Yield_Load~Taxon*Length*Width*Depth*Orient*Occlusion))
                        Df Sum Sq Mean Sq F value  Pr(>F)
Taxon                    3   6020    2007   2.641 0.05378 .
Length                   1   3781    3781   4.976 0.02802 *
Width                    1   7417    7417   9.762 0.00236 **
```

```
Depth                          1    133     133   0.174 0.67717
Orient                         1     47      47   0.062 0.80352
Taxon:Length                   3   8741    2914   3.834 0.01217 *
Taxon:Width                    3   2414     805   1.059 0.37022
Length:Width                   1     33      33   0.043 0.83550
Taxon:Depth                    3   1628     543   0.714 0.54594
Length:Depth                   1   2463    2463   3.242 0.07491 .
Width:Depth                    1    711     711   0.935 0.33597
Taxon:Orient                   3   8144    2715   3.573 0.01684 *
Length:Orient                  1   2647    2647   3.484 0.06502 .
Width:Orient                   1    517     517   0.680 0.41155
Depth:Orient                   1   1768    1768   2.327 0.13043
Taxon:Length:Width             3   6959    2320   3.053 0.03218 *
Taxon:Length:Depth             3   4022    1341   1.764 0.15915
Taxon:Width:Depth              3   8061    2687   3.536 0.01762 *
Length:Width:Depth             1    570     570   0.750 0.38861
Taxon:Length:Orient            3   1645     548   0.722 0.54135
Taxon:Width:Orient             3   4473    1491   1.962 0.12484
Length:Width:Orient            1      0       0   0.000 0.98698
Taxon:Depth:Orient             3    976     325   0.428 0.73318
Length:Depth:Orient            1   3190    3190   4.198 0.04319 *
Width:Depth:Orient             1   2356    2356   3.101 0.08144 .
Taxon:Length:Width:Depth       3   5861    1954   2.571 0.05867 .
Taxon:Length:Width:Orient      3   1736     579   0.762 0.51827
Taxon:Length:Depth:Orient      3   1787     596   0.784 0.50588
Taxon:Width:Depth:Orient       3   3293    1098   1.445 0.23464
Length:Width:Depth:Orient      1   1220    1220   1.605 0.20821
Taxon:Length:Width:Depth:Orient 3   5762    1921   2.528 0.06191 .
Residuals                     96  72945     760
---
Signif. codes:  0 ‘***’ 0.001 ‘**’ 0.01 ‘*’ 0.05 ‘.’ 0.1 ‘ ’ 1
> summary(aov(Yield_Load~Taxon:Length:Width:Depth:Orient:Occlusion))
                                    Df Sum Sq Mean Sq F value Pr(>F)
Taxon:Length:Width:Depth:Orient:Occlusion   8  17265    2158   2.115 0.0376 *
Residuals                                 151 154057    1020
---
Signif. codes:  0 ‘***’ 0.001 ‘**’ 0.01 ‘*’ 0.05 ‘.’ 0.1 ‘ ’ 1
```

Table 2. Summary statistics for printed shells.

```
summary(aov(Peak_Load~Taxon+Shell))
            Df Sum Sq Mean Sq F value   Pr(>F)
Taxon        1   1917    1917   1.427    0.236
Shell        3  84666   28222  21.005 2.84e-10 ***
Residuals   85 114202    1344
---
Signif. codes:  0 ‘***’ 0.001 ‘**’ 0.01 ‘*’ 0.05 ‘.’ 0.1 ‘ ’ 1
```

```
> summary(aov(Peak_Load~Taxon*Shell))
             Df Sum Sq Mean Sq F value   Pr(>F)
Taxon         1   1917    1917   1.559   0.2153
Shell         3  84666   28222  22.952 6.98e-11 ***
Taxon:Shell   3  13376    4459   3.626   0.0164 *
Residuals    82 100826    1230
---
Signif. codes:  0 ‘***’ 0.001 ‘**’ 0.01 ‘*’ 0.05 ‘.’ 0.1 ‘ ’ 1
> summary(aov(Peak_Load~Taxon:Shell))
             Df Sum Sq Mean Sq F value   Pr(>F)
Taxon:Shell   7  99959   14280   11.61 3.62e-10 ***
Residuals    82 100826    1230
---
Signif. codes:  0 ‘***’ 0.001 ‘**’ 0.01 ‘*’ 0.05 ‘.’ 0.1 ‘ ’ 1
>
> ##
> summary(aov(Yield_Load~Taxon+Shell))
             Df Sum Sq Mean Sq F value   Pr(>F)
Taxon         1   3180    3180   2.904    0.092 .
Shell         3  52477   17492  15.975 2.54e-08 ***
Residuals    85  93075    1095
```